Fabrication of Novel Potentiometric Sensor for Lead Ion Detection in Blood Samples: Experimental and Theoretical Approaches

Rezvan Moghaddasi [a], Majid Rezayi [b,c,d,*], Mahdieh Darroudi [d,e], Amirhossein Sahebkar [d], Fateme Haghiralsadat [a,f,*]

[a] Department of Advanced Medical Sciences and Technologies, School of Paramedicine, Shahid Sadoughi University of Medical Sciences, Yazd, Iran
[b] Medical Toxicology Research Center, Mashhad University of Medical Sciences, Mashhad, Iran
[c] Metabolic Syndrome Research Center, Mashhad University of Medical Sciences, Mashhad, Iran
[d] Department of Medical Biotechnology and Nanotechnology, Faculty of Medicine, Mashhad University of Medical Sciences, Mashhad, Iran
[e] Department of Physiology, Faculty of Medicine, Mashhad University of Medical Science, Mashhad, Iran
[f] Medical nanotechnology & tissue engineering research center, Yazd reproductive sciences institute, Shahid sadoughi university of Medical Sciences, Yazd, Iran

ARTICLE INFO

ABSTRACT

One of the significant health problems in some developing countries such as Iran is lead toxicity. Potentiometric plasticizer-free Pb^{2+} selective electrode based on a simple and biocompatible ionophore, curcumin, for lead (II) detection in erythrocytes have been developed. Glassy carbon electrode modification was done with curcumin as an ionophore. Curcumin and its interaction with lead (II) were characterized using FT-IR, FE-SEM, and UV–Vis spectroscopic techniques. Match potential method (MPM) was applying for determining selectivity coefficients of the proposed sensor. Furthermore, the structures were optimized in various media for both tautomeric structures of curcumin, and then the binding mechanism was supported by DFT calculation, being in a high correlation and agreement by experiment. Also, noncovalent interaction studies were done to obtain a description of the sensing process. The fabricated ISE based on photocurable self-plasticizing (n-butylacrylate) membrane with curcumin shows a potentiometric response with a Nernstain slop of 28.348 ± 0.68 mV per decade in a linear range from 1.0×10^{-9} to 1.0×10^{-2} and detection limit of 3.98×10^{-10} M. The sensor' s response time was about 20 s at room temperature. The sensor shows a sensitive detection of Pb^{2+} in human erythrocytes and standard solutions.

1. Introduction

With the rapid development of modern industries, lead is ubiquitous in the natural environment as one of the most toxic heavy metals due to their nonbiodegrability and accumulation in organisms [1–3]. Lead could be absorbed by humans and other organism and would lead to serious health including lungs, gastrointestinal tract, and even skin [2,4–6]. There are different published references for lead in the human body. One research reported that the maximum amount of lead is 70 µg/L for women, 90 µg/L for men (18–69 years old), and 35 µg/L for children 13–14 years old [7]. The MAK committee recommends setting the blood lead content of men and women over 45 to 300 µg/L as a safe value for occupational exposure [8].

Lead exposure is closely related to various harmful effects, among which the reproductive organs, kidneys, nervous and hematopoietic system, and cardiovascular system are the most critical targets [9].

Another result of lead exposure is impaired cognitive and intellectual abilities, acute encephalopathy, foot drop, wrist drop, muscle weakness, headache, insomnia, fatigue, seizures, anemia, and coma [10,11]. A study in Iran showed that lead exposure, even at a low level, might be a risk factor for pregnancy hypertension and preeclampsia in those who don't have any occupational exposure [12,13].

Many researchers have shown great attention in the past decade in the development and application of ion selective sensors [14]. New ionophores in construction of ion selective electrodes have been extensively studied. Many analytical techniques, such as inductively coupled plasma mass spectrometry, absorption spectrometry, and atomic fluorescence spectroscopy would be utilized for quantitatively analyze lead ions. However, these procedures have been limited to the laboratory due to the high cost of the appropriate equipment and the requirement for professional user [15]. In contrary, potentiometric sensors are being characterized using simple operation, fast response, nontoxic operation,

---

low cost, besides being suitable for online monitoring and outdoor operations of lead in aqueous [15,16]. For potentiometric sensors or ion selective electrodes (ISEs), ionophores embedded in the sensing membrane determine the sensitivity and selectivity of the sensor toward lead ion. While various ionophores have recently been developed for the coordination of lead ion selectively including calixarenes, crown ethers, nitrogen-containing compounds, and some O/S atom enriched organic molecules. Curcumin [1,7-bis (4-hydroxy-3methoxyphenyl)-1, 6-hepta-diene-3, 5-dione], and its derivatives have many applications, such as anticancer, antioxidation, antiinflammatory, antiatherosclerosis, delivery applications, and even scavenging free radical molecules in animal models [17]. One of the key roles of curcumin that has recently attracted attention is its sensory application as an ionophore to detect many cations and anions, such as Hg^{2+}, Fe^{2+}, Re^{2+}, Cu^{2+}, Pt^{2+}, S^{2-}, F^- and CN^-. The keto-enol isomerization of curcumin in 1,3-diketone can be chelated and finally form a complex with heavy metal ions (Scheme 1) [16].

The construction of ISE membrane is widely used for determining of lead ion in various environmental, industrial, and biochemical samples. Nevertheless, it made many problems when utilized for fabrication of solid-state sensors due to its poor adhesion on solid substances by solvent casting procedure. The addition of plasticizers to make it flexible causes its leaking into the solution during measurement and make it the main cause of toxicity, a specific environmental concern [18,19]. Therefore, these challenges would be resolved with the sue of self-plasticizing and photocurable polymer technique[20].

Here, we designed a novel potentiometric sensor based on curcumin ionophore, which uses a self-plasticizing method to detect lead in human erythrocytes, showing high selectivity to Pb^{2+} over different kinds of cations. This sensor was faster, easier, and even cheaper than the previously mentioned methods. So far, there has not been any report on the self-plasticization method of Pb^{2+} -ISE based on curcumin. The fabricated potentiometric sensor in this study was used for lead (II) detection in human erythrocytes.

2. Method

2.1. Materials and methods

The materials used in membrane fabrication like 2-hydroxyethyl methacrylate (HEMA), 2,2-dimethoxy-2-phenyl acetophenone (DMPP), n-butyl acrylate (n-BA), 2-hexane-diol diacrylate (HDDA), Curcumin, and Sodium tetrakis (4-chlorophenyl) borate (NaTFPB), were bought from Sigma-Aldrich. The metal ions salts used such as $Pb(NO_3)_2$, $ZnCl_2$, $NiCl_2$, $MgCl_2$, $CaCl_2$, NH_4Cl, $NaCl$, and KCl were purchased from Merck company. Also, the $CuCl_2$ and Triton X-100 were purchased from Fluky and Scharlau, respectively. All other solvents and chemicals throughout this study were purchased from Merck Company and used as received in reagent grade.

2.2. Instruments

A digital pH/ISE meter (Orion Star A214) was used to measure the difference in potential (electromotive force) of the fabricated sensor. The reference electrode was an Ag-AgCl double-junction electrode (3.0 M NaCl internal solution, BASi, USA). The Infrared spectra (IR) of samples were recorded between 4000 and 400 cm^{-1} as an attenuated total reflectance (ATR) on a Thermo Nicolet AVATAR 370 FT-IR

spectrometer. The spectrophotometer type UV/Vis/NIR (UV- 3600 Shimadzu) equipped with temperature controller TCC-2 was utilized to get the spectra of curcumin ionophore, Pb^{2+} their complexes. Field Emission Scanning Electron Microscope Tescan equipped with Energy Dispersive facility (FESEM-EDX) was used to analyze the morphology of the membrane.

2.3. Membrane preparation:

The photocuring technique was applied for preparing the membrane sensor according to the previously reported method [19,21,22]. An inner layer consisting of 98.40 wt% HEMA as a monomer and 1.60 wt% DMPP as a photoinitiator. The mixture was sonicated to form a homogenous mixture. 0.1 μL of the mixture dropped casted onto the GCE and polymerized by using UV box with a constant flow of nitrogen gas for 480 s. The polymerized inner layer of the membrane was then dipped with 0.01 M Pb^{2+} for 18 min. The outer layer of the membrane was prepared by mixing 3.80 wt% Cur, 1.40 wt% DMPP, 0.10 wt% HDDA, 0.90 wt% NaTFPB and 94.40 wt% n-BA. 2.0 μL of the mixture is then dropped onto the hydrated poly-(HEMA) inner layer and photocured for 360 s.

2.4. Complexation study

In order to study primary complexation between Pb^{2+} and curcumin ionophore, absorption spectra of three solutions (1.0 × 10^{-5} M of curcumin ionophore, 1.0 × 10^{-4} M of Pb^{2+}, and their mixture in 1:1 V/V) was carried out spectrophotochemically by using UV- 3600 Shimadzu spectrometer over a range of 200–600 nm [23]. Titration between 1.0 ml of curcumin ionophore (1.0 × 10^{-5} M) and 1.0 × 10^{-4} M of Pb^{2+} (1.0 × 10^{-4} M) at 25 °C in the EtOH-DI-water (1:1) was conducted to study the stoichiometry of formed complex between curcumin ionophore and 1.0 × 10^{-4} M of Pb^{2+} by using UV–Vis. The spectra were recorded in the range of 200 nm to 600 nm at 2 min after each addition [24].

2.5. Sensor evaluation

Potential measurements were carried out in an electrochemical cell setup containing a double junction Ag/AgCl reference electrode. The inner reference solution was 0.1 M Tris-HCl (pH = 7), whereas 1 M lithium acetate was utilized as a gel bridge electrolyte. Then, the Ag/AgCl reference and modified GCE working electrode were connected to an Orion meter. All test solutions of $Pb(NO_3)_2$ in a concentration range of 10^{-10}-10^{-1} M were prepared in DI water [25]. All of these measurements were done at room temperature.

2.6. Computational study

The Gaussian-09 program package was used for all calculations [26]. Geometry optimization of all compounds is performed with the gradient-corrected DFT level coupled with the hybrid exchange–correlation functional [26]. It uses the Coulomb-attenuating method with B3LYP/6–311++G(2d,2p) level of theory, which was found to be suitable for the whole molecule without any asymmetry restrictions in the ground state (GS) [27,28]. The effect of solvent was estimated by the conductor-like polarizable continuum model (CPCM) calculations in Gas-phase, H_2O, Methacrylate, and the mixed solvent of H_2O: Methacrylate (1:1) [29–32]. The reported energies are Gibbs free energies,
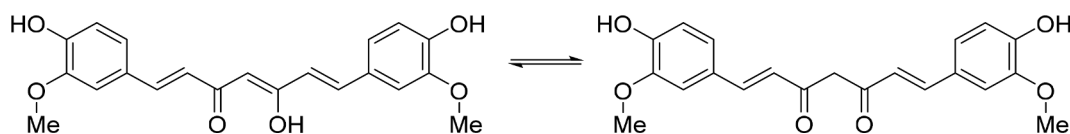
Scheme 1. Enol-Keto structures of Curcumin ionophore.

which contain zero-point vibrational corrections, thermal and entropy corrections at 298 K, and solvation energies. The noncovalent interaction (NCI) topological analysis was also performed on the prepared complex with the MultiWfn [33].

3. Results and discussion

3.1. Computational study on the sensing mechanism

The metal complexes structures, (1:1) and (1:2) ratio stoichiometries of curcumin in different tautomer structures were optimized without restriction in the gas phase and in the solvent medium under optimization conditions by using the PCM model in water, methacrylate media, and water: methacrylate media. It was predicted using the DFT method to better understand the process, which took place between Pb and curcumin during complexation. The optimized structure of curcumin and its tautomer are shown in Fig. 1. The tautomeric structure of curcumin and their Pb-complexes are displayed in the enol-keto tautomer, which forms non-conjugated fragments, while in enol structure, it is a linear conjugated system. As shown in Fig 9, the energies of each tautomeric isomers in various solvents are displayed. It is clear that the enol structure of curcumin and the (1:1) and (2:1) Pb complexes are more stable than the keto structures. Also, it was demonstrated that all the optimized structure in the water environment is the most stable configurations and the stabilities of these structures in different environments are respectively $H_2O > H_2O$: Methacrylate (1:1) > Methacrylate > Gas-phase. The relative energies of the tautomer enol-keto are collected in Table 1. As exhibited in Table 1, the solvent's alteration led to a slight reduction of the energy gap and more substantial relatives Gibbs free energy.

Based on the most stable of the optimized structure by using the PCM model in the water environment, we consider other calculations based on water. The keto tautomer structure consists of separate fragments shown in the electron cloud in the HOMO keto form of curcumin and its complexes. The electron clouds are mainly distributed on one fragment of the curcumin structure. In contrast, the electron density of HOMO in the enol form of curcumins' derivatives delocalized on the whole molecule (Fig. 1g). Also, it was exhibited that the HOMO-LUMO bandgaps of keto structures are much more than the enol form of curcumin, and the HOMO-LUMO bandgap of curcumin and tautomer structure of curcumin become smaller for four various complexes. Accordingly, the decreasing bandgap energy was seen because of the adsorption of Pb^{2+} and the charge transfer.

Fig. 2. The FMO analysis of (a) enol-Curcumin, (b) keto-Curcumin,

		ΔG_{rel} (kcal/mol)
E_{gas} = -1262.978	E_{gas} = -1262.965	-8.15
E_{met} = -1262.993	E_{met} = -1262.983	-6.27
$E_{Met:water}$ = -1263.006	$E_{Met:water}$ = -1262.992	-8.78
E_{water} = -1263.008	E_{water} = -1263.001	-4.39
(a)	(b)	
E_{gas} = -1418.390	E_{gas} = -1418.331	-37.02
E_{met} = -1418.404	E_{met} = -1418.343	-38.27
$E_{Met:water}$ = -1418.510	$E_{Met:water}$ = -1418.475	-21.96
E_{water} = - 1418.513	E_{water} = -1418.479	-21.33
(c)	(d)	

Fig. 1. The optimized structure and Energies of (a) enol-Curcumin, (b) keto-Curcumin, (c) enol-Curcumin: Pb (1:1), (d) keto-Curcumin: Pb (1:1), (e) enol-Curcumin: Pb (2:1), and (f) keto-Curcumin: Pb (2:1) in Hartree, and the relative energies in gas phase, water, methacrylate media, and water: methacrylate, and (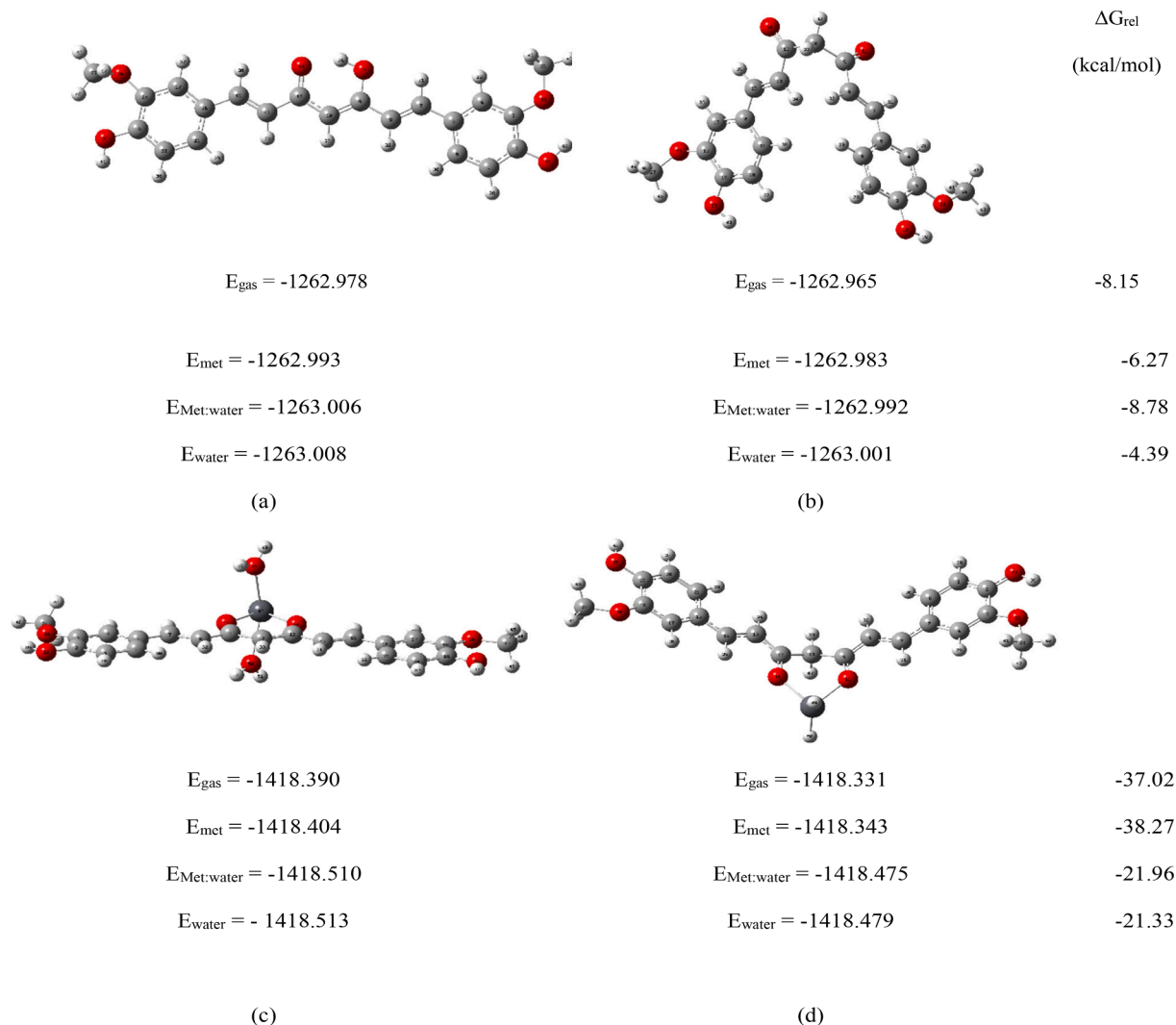g) The FMO analysis of (a) enol-Curcumin, (b) keto-Curcumin, (c) enol-Curcumin: Pb (1:1), (d) keto-Curcumin: Pb (1:1), (e) enol-Curcumin: Pb (2:1), and (f) keto-Curcumin: Pb (2:1) in eV.
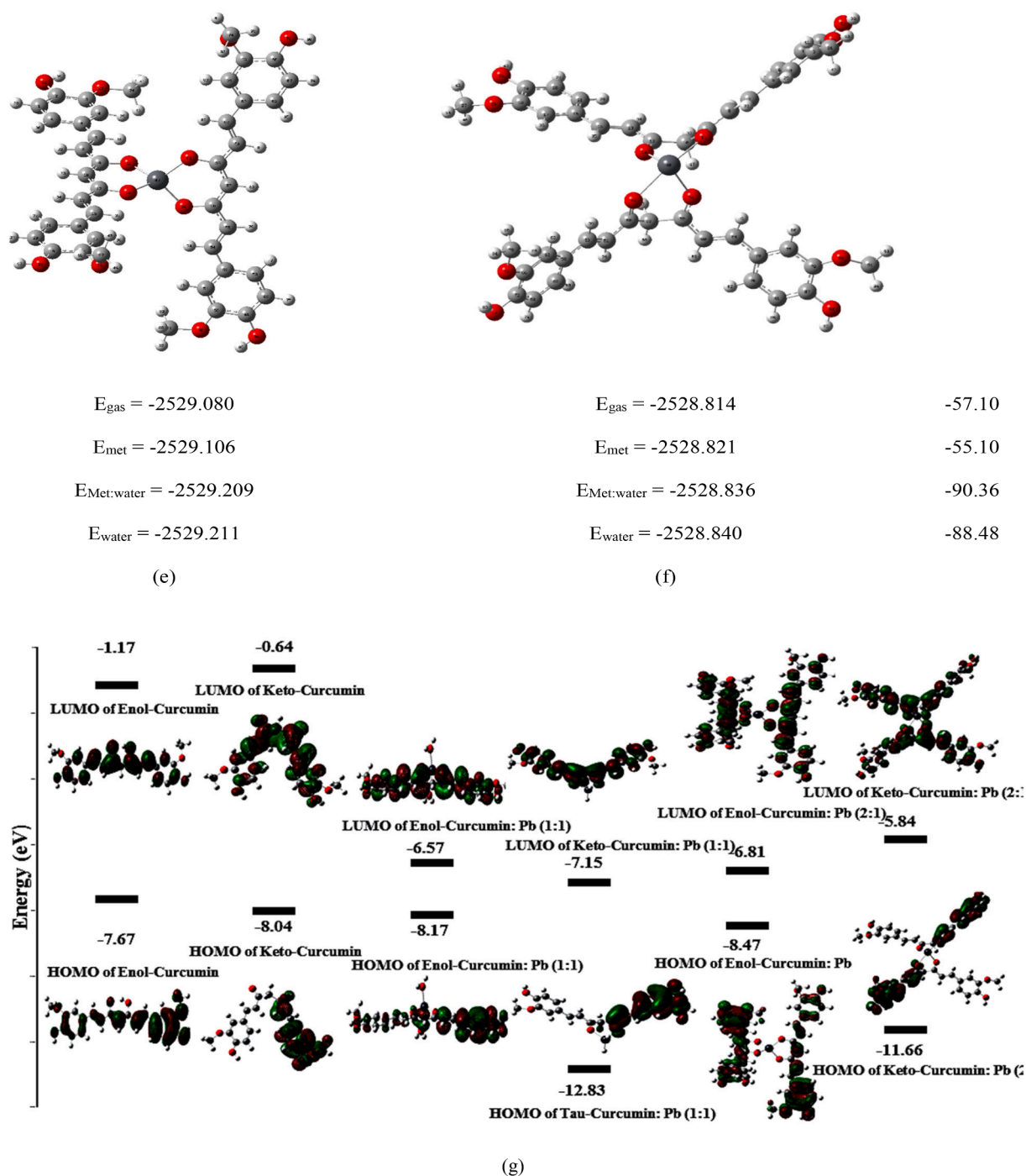
$E_{gas} = -2529.080$	$E_{gas} = -2528.814$	-57.10
$E_{met} = -2529.106$	$E_{met} = -2528.821$	-55.10
$E_{Met:water} = -2529.209$	$E_{Met:water} = -2528.836$	-90.36
$E_{water} = -2529.211$	$E_{water} = -2528.840$	-88.48
(e)	(f)

(g)

Fig. 1. (*continued*).

(c) enol-Curcumin: Pb (1:1), (d) keto-Curcumin: Pb (1:1), (e) enol-Curcumin: Pb (2:1), and (f) keto-Curcumin: Pb (2:1) in eV.

The further characterization on interactions described above has been performed by NCI plot index for both keto-enol tautomer structures of curcumin and their (1:1) and (2:1) complexes (Fig. S1). The NCI plot isosurface analysis confirms the more overlap of the π system since the green isosurface extends from one end to the other of the conjugated system.

The reactivity descriptors based on DFT also have been used to describe the reactivity, charge transfer, and stability by Koopman's theory equations. The means of HOMO-LUMO energies value is established as electronic chemical potential as $\mu = (E_{LUMO} + E_{HOMO})/2$, and also the global electrophilicity is defined the charge transfer process as

$\omega = \mu_2/2\eta$. Moreover, the chemical hardness in the HOMO-LOMO bandgap differences as $\eta=(E_{LUMO}-E_{HOMO})$. The higher amount of μ and energy gap HOMO-LOMO demonstrated higher kinetic stability. The resistance to deformation of the electron cloud was signified with a higher hardness under small perturbations. As exhibited in Table 1, the highest relative μ is related to the enol form of curcumin. The highest amount of electrophilicity is found to be in the (1:1) and (2:1) complexes of enol-curcumin. The lower gap for complex represents the softer system along with higher electrophilicity indices.

In order to establish a comparison between the stability of Curcumin-Pb complexes for both enol-keto tautomer structures, the calculated binding energies for complexes are listed in Table 1. It is revealed a stronger interaction between the enol-Curcumin and Pb^{2+} in the (2:1).

Table 1

The calculated electronic chemical potential μ, chemical hardness η, global electrophilicity ω indices, the HOMO and LUMO energies gap in eV, and the changes in binding energy E, enthalpy H, and Gibbs free energy G in water environment kJ mol for Curcumin, Tautomeric structure of curcumin, (1:1) complex, Tautomeric structure of Curcumin: Pb (1:1), (2:1) complex, and Tautomeric structure of Curcumin: Pb (2:1), and.

Entry	μ	ω	η	$\Delta E_{HOMO-LUMO}$	ΔE	ΔH	ΔG
Enol-Curcumin	−4.3	1.5	12.9	6.49	–	–	–
Keto-Curcumin	−4.4	1.2	14.8	7.40	–	–	–
Enol-Curcumin: Pb (1:1)	−7.3	17.0	3.2	1.60	196.9	196.3	205.7
Keto-Curcumin: Pb (1:1)	−9.9	8.8	11.3	5.68	166.9	166.9	178.8
Enol-Curcumin: Pb (2:1)	−7.6	17.6	3.3	1.66	316.5	316.1	339.6
Keto-Curcumin: Pb (2:1)	−8.7	6.6	11.6	5.82	233.8	234.7	245.7

The binding energy for complexes of curcumin toward Pb^{2+} ion diminished for (2:1) complex. So, it could be predicted that (2:1) stoichiometric ratio for Pb^{2+} and the enol form of curcumin could be regarded as the most favorable interactions.

3.2. UV–Vis analysis

The complexation study between curcumin and Pb^{2+} was done by UV–Vis spectroscopy. The results are shown in Fig. 2 (I). As seen, Pb($NO_3)_2$ spectra show a maximum absorption peak at 210 nm, but the spectra of curcumin show maximum absorption peaks at 200 and 431 nm. After adding Pb^{2+} solution to curcumin, distinct spectral changes were included, and the intensity of curcumin peak at 431 nm decreased [17]. These significant changes indicate that the selective complexion between Pb^{2+} and curcumin ionophore occurred.

To assess the interacting potential of curcumin and Pb^{2+}, the UV–Vis titration experiment was carried out, and also the stoichiometry of the complex between curcumin and Pb^{2+} cation was measured. As represented in Fig. 2 (II). By increasing the molar fraction of Pb^{2+}, curcumin absorption spectra gradually decrease. This result demonstrates a stoichiometry of 2:1. (inset of Fig. 2 (II)) for the plot of absorbance versus the molar ratio of $[Pb^{2+}]/[CUR]$. Thus, the suggested process for the CUR-Pb^{2+} complex is (Eq. 1):

$$Pb^{2+} + 2curcumin \leftrightarrow 2curcumin - Pb^{2+} \quad (1)$$
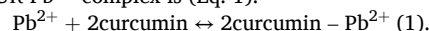
Eventually, it can result in the determination of the amount of Pb2 + ions in a solution by using the proposed sensor. The detection limit of curcumin toward Pb^{2+} was determined to be 38 μM with a linear range of concentration to be 0–3 μM.

3.3. Study of electrode composition

The performance of membrane sensors is affected by so many parameters such as membrane composition, ionophore amount, additive amount, pH effect, interference effect, and the lifetime of the sensor. The composition of the membrane sensor was varied to reach the optimum amount found in determining the target of interest. In this study, in

(I)

(II)

(III)
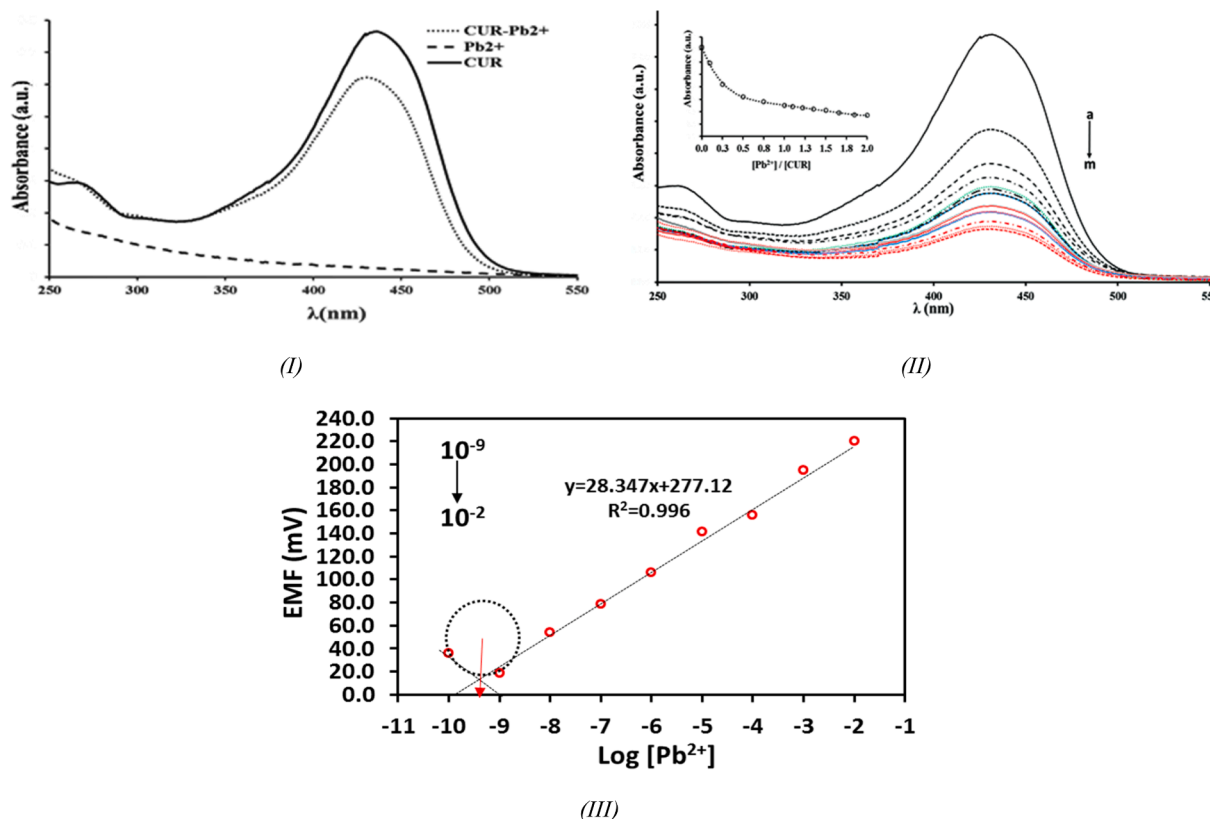
Fig.2. (I) UV–Visible spectra of 1.0×10^{-4} M Pb($NO_3)_2$, 1.0×10^{-4} M curcumin ionophore, and their mixture 1:1 (V/V)., (II) UV–Vis spectra of (a) 1.0×10^{-5} M Pb^{2+}, (b) 1.0×10^{-5} M CUR and (c) mixture of CUR ionophore and Pb^{2+} cation (1:1, v/v), and UV–Vis absorption spectra of CUR ionophore (1.0×10^{-5} M) in 1:1 DI: EtOH mixture in the presence of an increasing concentration of Pb^{2+} and absorbance versus the $[Pb^{2+}]/[CUR]$ molar ratio and plots., and (III) Calibration graphs of lead (II) self-plasticizing CUR-based membrane GCE.

order to reach the optimum amounts of membrane composition, 10 membrane sensors with different amounts of ionophore and additive were prepared and tested in the concentrations of Pb^{2+} in the range of 1.0×10^{-10} to 1.0×10^{-1} M (Table 2). In preliminary studies, the self-plasticizing membranes with and without CUR ionophore were constructed and exhibited the Nersntian and narrow response toward the lead (II) ions, respectively. In self-plasticizing membrane sensors, the ionophore as a key element of the membrane should be an optimum amount to get the Nernstaian response at the membrane-bulk solution interface, which is owing to the membrane potential. Also, the amount of NaTFPB additive used in the membrane composition significantly influenced the selectivity and sensitivity of the self-plasticizing membrane sensor. In comparison with other lead PVC-based membrane sensors, the use of the self-plasticizing polymer was found to enhance the detection limit and stability of the potential response of the sensor.

Fig. 2 (III) represents the significant enhancement of the potential slope of the self-plasticizing polymeric membrane modified GCE based on CUR ionophore with a Nernstan slope of 28.34 mV/decade for the lead (II) cation over the working range of 1.00×10^{-9} to 1.00×10^{-2} M with detection limit 3.98×10^{-10} M. The IUPAC recommendation was used for evaluation of working range of concentration and detection limit of the proposed sensors.

In order to assay fabricated ion sensor for detecting lead (II) in human Red Blood Cell (RBC), the whole blood specimen was at first centrifuged to access RBC because the majority of lead is taken up into RBC. RBC specimen was vortex for 5 min to create homogeneity. Then, the small RBC volume was extracted from the whole specimen. It diluted 1 in 100 with DI water containing ammonia, Na_2EDTA, and triton x-100 [1]. Then we spike different concentrations of $Pb(NO_3)_2$ solution in diluted RBC to examine if the protein and other ions in the blood affect our ISE detection of lead (II) or not.

3.4. Characterization of optimized electrode

The FTIR spectrum of curcumin, optimized membrane, and complex of curcumin-Pb^{2+} is shown in Fig. 3 (I). For curcumin, the bands that are seen at 3505 cm^{-1}, 1628 cm^{-1}, 1509 cm^{-1}, 1282 cm^{-1}, and 1154 cm^{-1} are ascribed to the phenolic –OH stretching, -C $=$ O group, -C $=$ C vibrations, aromatic –C-O stretching, and C-O-C stretching modes, respectively. It can be seen in the figure that the prominent absorption peak was seen just for the optimized membrane. This result illustrates that the polymer covers the curcumin moiety. After interaction with lead (II), there was a shift in –OH group from 3505 cm^{-1} to 3501 cm^{-1} that there wasn't seen before. Also, the percentage of transmittance for the peak 1628 cm^{-1} was changed after detecting Pb^{2+}. These results proved that –OH and C $=$ O groups are taking part in forming the complex between curcumin and lead (II). The peaks 575 and 543 cm^{-1} vanished in the complex spectrum, indicating that curcumin and lead (II) successfully form a complex with each other.

FESEM characterization was done on the surface of the fabricated sensor to study the morphology of ISE before and after the destocking of fresh membrane into $Pb(NO_3)_2$ solutions. Fig. 3(II). clearly shows the cluster of Pb^{2+} atoms on the surface of curcumin. It means that the complex of curcumin and Pb^{2+} occurred.

The EDX analysis was done in order to determine the complex formation between Pb^{2+} and curcumin. The spectrum of the optimized membrane after adding $Pb(NO_3)_2$ solution is displayed in Fig. S2. The attendance of Pb^{2+} in the membrane shows the complex between curcumin and Pb^{2+} successfully occurred.

3.5. Determination of selectivity coefficient

The match potential method (MPM) was used to evaluate the selectivity of the self-plasticizing GCE based on CUR ionophore [34]. According to IUPAC recommendation, for calculation of selectivity coefficient, $logK_{Pb,j}^{MPM}$ the known concentration of lead (II) ion solution ($a'_{Pb^{2+}} = 1.00 \times 10^{-1}$ M) was added to the reference solution based on the fixed concentration of thiocyanate ions ($\alpha_{Pb^{2+}}=1.00 \times 10^{-6}$ M), and the change in potential was recorded (Eq. 2). In parallel, the same way was followed for each interfering cations by adding their known concentration to the reference solution to obtain the same potential change as before. The selectivity coefficient factors were calculated for each interfering cations by using the following equation:

$$logK_{Pb,j}^{MPM} = \frac{(a'_{Pb^{2+}} - a_{Pb^{2+}})}{a_B} \text{ (2)}.$$

Table 3 presented the compression of selectivity coefficients for the optimized self-plasticizing CUR-based membrane GCE. The concluded results showed the strong affinity of the proposed membrane sensor to lead (II) in compression of all tested foreign cations. This result displays those other common cations in human blood cannot significantly interfere with fabricated lead (II) sensor in this work.

3.6. Response and lifetime of the optimized electrode

Another essential feature of a sensor is its response time. An efficient ISE should generate both stable and reproducible potential in a short response time (the first moment at which the potential of the cell reaches the 95% steady value within $\pm$ 1 mV after the work and the reference electrode are placed into the sample solution) [24]. Fig. 4 (I). Shows the response time of fabricated electrode in various concentrations of Pb $(NO_3)_2$ from 1.00×10^{-9} to 1.00×10^{-2} M, and the sensor's response time was close to 20 s. The potentiometric response of the proposed electrode and plotting its calibration curve were recorded for time. The lifetime of fabricated- ISE was about 4 weeks and swelled up due to leaching membrane ingredients into the solution.

Table 2

Composition, slopes, linear ranges, and detection limits of calibration curves for lead (II) self-plasticizing CUR-based membrane GCE.

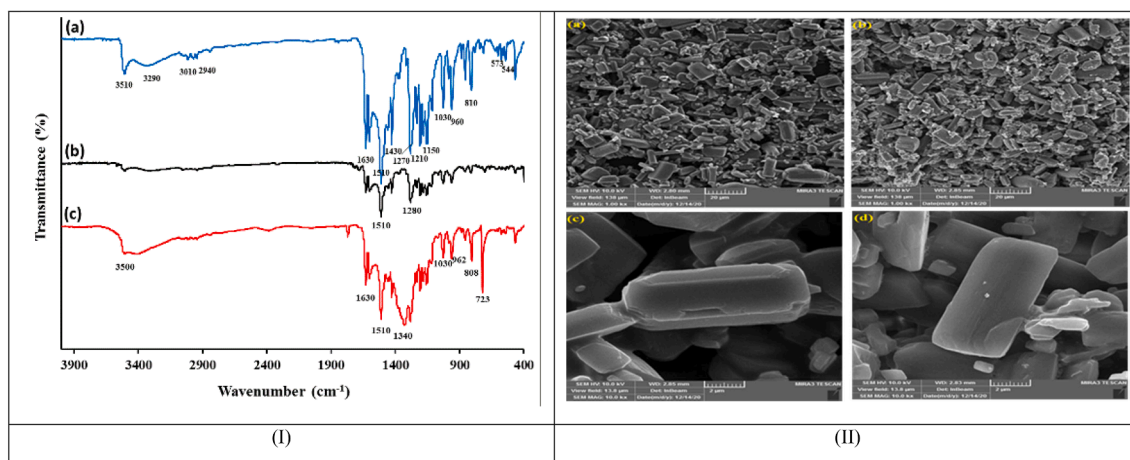| ELC NO.	LINEAR RANGE (M)	SLOPE (MV/DEC)	DMPP* (WT.%)	HEMA (WT.%)	NATFPB (WT.%)	CUR (WT.%)	DMPP** (WT.%)	HDDA (WT.%)	N-BA (WT.%)	R^2
E1	$1.0 \times 10^{-10} - 1.0 \times 10^{-1}$	11.3 ± 0.97	1.60	98.00	0.80	0.00	1.00	0.10	95.50	0.98
E2	$1.0 \times 10^{-9} - 1.0 \times 10^{-2}$	28.34 ± 0.68	1.60	98.6	1.20	3.60	1.20	0.10	94.40	0.99
E3	$1.0 \times 10^{-6} - 1.0 \times 10^{-2}$	21.8 ± 0.34	3.00	90.00	1.00	1.00	1.50	0.10	98.00	0.97
E4	$1.0 \times 10^{-6} - 1.0 \times 10^{-2}$	23.5 ± 0.26	2.70	90.00	1.20	3.50	1.10	0.10	94.40	0.98
E5	$1.0 \times 10^{-6} - 1.0 \times 10^{-1}$	22.75 ± 0.19	3.00	90.00	0.50	4.10	1.60	0.50	90.00	0.99
E6	$1.0 \times 10^{-5} - 1.0 \times 10^{-1}$	24.23 ± 0.17	1.60	98.6	1.20	3.50	1.20	0.10	94.40	0.99
E7	$1.0 \times 10^{-8} - 1.0 \times 10^{-1}$	33.68 ± 0.97	3.00	90.00	0.50	4.00	1.60	0.50	90.00	0.99
E8	$1.0 \times 10^{-6} - 1.0 \times 10^{-2}$	21.05 ± 0.24	1.60	98.00	0.00	3.60	1.10	0.10	95.50	0.99
E9	$1.0 \times 10^{-6} - 1.0 \times 10^{-1}$	18.88 ± 0.23	1.60	98.00	1.10	4.00	1.10	0.10	94.10	0.99
E10	$1.0 \times 10^{-8} - 1.0 \times 10^{-1}$	23.25 ± 0.27	1.60	98.00	1.50	4.30	1.10	0.10	94.10	0.99

* Inner Layer.
** Outer layer.

Fig. 3. Comparison of (I) FT-IR spectra for (a) CUR ionophore, (b) fabricated membrane and (c) used membrane in 1×10^{-2}M lead (II) nitrate solution. (II) FESEM micrographs of the optimized fresh membrane (a,c) and optimized membrane after destocking into the $Pb(NO_3)_2$ solutions (b,d).

Table 3
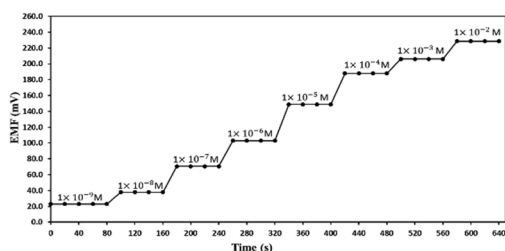The selectivity coefficient of various interfering cations for the membrane sensor.

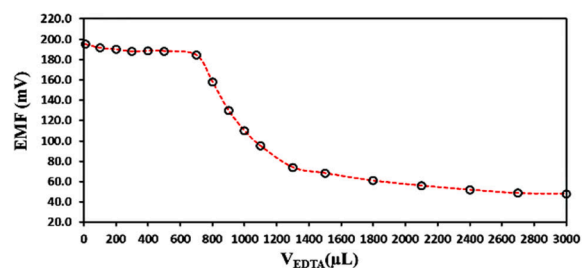| Interference Ions	a_B	$a'_{Pb^{2+}}$	$\dfrac{(a'_{Pb^{2+}} - a_{Pb^{2+}})}{a_B}$	$logK_{Pb,j}^{MPM}$
Ni^{2+}	4.20×10^{-3}	1.10×10^{-5}	2.30×10^{-3}	-2.60
K^+	3.20×10^{-3}	1.10×10^{-5}	3.10×10^{-3}	-2.50
NH_4^+	3.00×10^{-3}	1.10×10^{-5}	3.30×10^{-3}	-2.42
Ca^{2+}	9.00×10^{-4}	1.10×10^{-5}	1.10×10^{-2}	-1.95
Zn^{2+}	6.00×10^{-4}	1.10×10^{-5}	1.60×10^{-2}	-1.69
Na^+	2.40×10^{-4}	1.10×10^{-5}	4.16×10^{-2}	-1.38
Mg^{2+}	4.00×10^{-5}	1.10×10^{-5}	2.50×10^{-2}	-0.60
Cu^{2+}	2.00×10^{-5}	1.10×10^{-5}	$5.0 \times '0^{-1}$	-0.30

3.7. Repeatability and reproducibility of ISEs

Repeatability of the fabricated sensor was performed by using identical ISE three times. The standard deviation (SD) for the repeatability test was 0.14, and the Coefficient of Variation (CV) was 0.6%. A reproducibility study was carried out by using five Pb^{2+}-ISEs in which each electrode was used just for one time. It was exhibited that the SD for the repeatability test was 0.58, and the CV was 2.5%. The difference in the Nernstain slope of five electrodes in the reproducibility test could be due to variation of thickness and morphology in each membrane of electrode compared to the other, which results in fluctuation of the extraction equilibrium of corresponding ions in the vicinity of the interface between the membrane and aqueous layer. As a result, the electrode membrane's thickness variation can create a minor change in ISE slope.

3.8. Titration of $Pb(NO_3)_2$ by EDTA

The proposed Pb^{2+}-ISE was effectively utilized as an indicator electrode in laboratory conditions. The potentiometric titration of 1.00×10^{-3} M (5 ml) was performed by EDTA (1.0×10^{-2}M) using the optimized electrode. As it can be seen from Fig. 4 (II), a standard sigmoidal shape with a sharp break point of titration curve indicates the selectivity of the fabricated sensor. Also, the endpoint of the curve corresponds to 1:2 stoichiometry of the EDTA-lead (II) complex. Before the endpoint, the potential show usual logarithmic changes by adding the volume of EDTA titration. After it, the potential stays approximately stable because of the low concentration of Pb^{2+} ions in the solution due to their complexation with EDTA.

3.9. Comparative study

The fabricated-ISE in this study with curcumin as ionophore was compared with the recently published Pb^{2+} selective electrode. As shown in Table 4, all the Pb^{2+}-ISEs studies had plasticizers in their membrane, while this work was applied in the self-plasticizing method. As seen proposed sensor is comparable with reported Pb^{2+}-ISEs in selectivity, response time, working concentration range. It can result that the proposed electrodes can be used effectively for accurate and precise detection of Pb^{2+} concentration in human blood.

The proposed Pb^{2+}-ISE was successfully used to detect different Pb^{2+} concentrations in real samples. From the results arranged in Table 5, the results of the recovery experiment performed in diluted whole blood samples with DI-water. For the recovery test, we applied the human whole blood samples of Pb^{2+} cations were spiked into the diluted human

Fig. 4. (I) Dynamic response time of the fabricated sensor in $Pb(NO_3)_2$ solutions in the concentration range of 1.00×10^{-9}-1.00×10^{-2} M, and (II) Potentiometric titration curve of 5 ml $Pb(NO_3)_2$ solution (1.00×10^{-3} M) with EDTA (1.00×10^{-2} M) based on the prepared sensor as an indicator electrode.

Table 4

comparison of the proposed Pb^{2+}-ISE in this study with the reported potentiometric sensor.

No.	Ionophore	Slope (mV/decade)	Linear range (M)	LOD(M)	Response time (s)	Ref.
1	Curcumin	28.34	*1.00×10^{-9}-1.00×10^{-2}*	3.98×10^{-10}	20	This study
2	Dibenzodiaza-15-crown-4	28.2	$5.00 \times 10^{-6} - 1.00\ 10^{-2}$	3.50×10^{-6}	15	[35]
3	1,2-bis(N'-benzoylthioureido)benzene	30.37 ± 0.62	$6.31 \times 10^{-8} - 3.98 \times 10^{-2}$	2.51×10^{-8}	15	[24]
4	Benzyl disulphide	29.2 ±1.3	$2.00 \times 10^{-5} - 5.00 \times 10^{-2}$	1.00×10^{-5}	240	[36]
5	5,5'-dithiobis-(2-nitrobenzoic acid)	29.00 ± 0.3	$4.00 \times 10^{-6} - 1.00 \times 10^{-2}$	4.00×10^{-6}	70	[37]
6	1,3-bis(N'-benzoylthioureido)benzene	31.5 ±1.6	$4.00 \times 10^{-6} - 1.00 \times 10^{-2}$	1.60×10^{-6}	10	[38]
7	Methylene Bis (diisobutyldithiocarbamate)	28.0	$1.00 \times 10^{-2} - 1.00 \times 10^{-6}$	1.60×10^{-7}	16	[39]
8	tetrakis(2-hydroxy-1-naphthyl)porphyrins	29.2 ± 0.3	$3.20 \times 10^{-5} - 1.00 \times 10^{-1}$	3.50×10^{-6}	10	[40]

Table 5

Comparison of fabricated Pb^{2+} ISE sensor in determining the Pb^{2+} concentration in spiked whole blood samples.

Sample No.	Pb^{2+} [a]Added (ppm)	Founded (ppm)	[b]Recovery	[c]RSD (%)
1	100	87.66	87.66	0.068
2	200	87.66	93.83	0039
3	300	962	97.33	0.125
4	500	496	99.2	0.218
5	700	663.33	94.7	1.57
6	1000	1013	101.3	0.332

[a] Average of three determination;

[b] Recovery = (found/added) × 100.

[c] RSD = (SD/average) × 100.

whole blood samples and were then detected by the presented proposed sensor. In spite of the complex fluid matrix, lead (II) cation was successfully detected with significant accuracy (Recovery%, 87.66 – 101.3) and acceptable precision (RSD%, 0.039– 1.57).

4. Conclusion

This paper has designed a simple potentiometric plasticizer-free Pb^{2+}-selective ISE based on curcumin as an ionophore. This sensor can solve the issue of requiring plasticizers in PVC-based membrane sensors. The response of the fabricated sensor to lead (II) revealed a low detection limit 3.98×10^{-10} M, in a concentration range of 1.0×10^{-9} to 1.0×10^{-2} M was in Nernstain slope of 28.347 ± 0.68 mV/decade with strong selectivity and rapid response time. The proposed Pb^{2+}-ISE was successfully used to detect different Pb^{2+} concentrations in real samples. Moreover, DFT and NCI gradient studies were implemented for the binding mechanism of the assessment of stoichiometry and behavior of both tautomeric structures of ionophores. It was exhibited that the enol structure is more stable than the keto structure. The experimental results and theoretical works beside each other could be used to develop and clarify sensing mechanisms.

Declaration of Competing Interest

The authors declare that they have no known competing financial interests or personal relationships that could have appeared to influence the work reported in this paper.

Appendix A. Supplementary data

Supplementary data to this article can be found online at https://doi.org/10.1016/j.microc.2022.107383.

References

[1] A. Schütz, I.A. Bergdahl, A. Ekholm, S. Skerfving, Measurement by ICP-MS of lead in plasma and whole blood of lead workers and controls, Occupational and environmental medicine 53 (11) (1996) 736–740.

[2] K. Klotz, T. Göen, Human biomonitoring of lead exposure. Lead-Its Effects on Environment and Health, De Gruyter, 2017.

[3] O. Mehrpour, P. Karrari, and M. Abdollahi, "Chronic lead poisoning in Iran; a silent disease," ed: Springer, 2012.

[4] E. Obeng-Gyasi, Sources of lead exposure in various countries, Reviews on environmental health 34 (1) (2019) 25–34.

[5] C.F. Delgado, M.A. Ullery, M. Jordan, C. Duclos, S. Rajagopalan, K. Scott, Lead Exposure and developmental disabilities in preschool-aged children, Journal of Public Health Management and Practice 24 (2) (2018) e10–e17.

[6] I. A. Bergdahl, A. Schütz, L. Gerhardsson, A. Jensen, and S. Skerfving, "Lead concentrations in human plasma, urine and whole blood," *Scandinavian journal of work, environment & health,* pp. 359-363, 1997.

[7] H. Roels, G. Hubermont, J. Buchet, R. Lauwerys, Placental transfer of lead, mercury, cadmium, and carbon monoxide in women: III. Factors influencing the accumulation of heavy metals in the placenta and the relationship between metal concentration in the placenta and in maternal and cord blood, Environmental research 16 (1–3) (1978) 236–247.

[8] C. Schulz, M. Wilhelm, U. Heudorf, M. Kolossa-Gehring, Update of the reference and HBM values derived by the German Human Biomonitoring Commission, International journal of hygiene and environmental health 215 (1) (2011) 26–35.

[9] P. M. Howard, "Occupational health and safety," *The Wiley Blackwell Encyclopedia of Health, Illness, Behavior, and Society,* pp. 1708-1712, 2014.

[10] M. Wang, F. Hossain, R. Sulaiman, X. Ren, Exposure to inorganic arsenic and Lead and autism Spectrum disorder in children: a systematic review and meta-analysis, Chemical research in toxicology 32 (10) (2019) 1904–1919.

[11] H.N. Karimooy, M.B. Mood, M. Hosseini, S. Shadmanfar, Effects of occupational lead exposure on renal and nervous system of workers of traditional tile factories in Mashhad (northeast of Iran), Toxicology and industrial health 26 (9) (2010) 633–638.

[12] M. Vigeh, et al., Lead and other trace metals in preeclampsia: a case–control study in Tehran, Iran, Environmental research 100 (2) (2006) 268–275.

[13] M. Vigeh, et al., Relationship between increased blood lead and pregnancy hypertension in women without occupational lead exposure in Tehran, Iran, Archives of Environmental Health: An International Journal 59 (2) (2004) 70–75.

[14] M. Boskabady, N. Marefati, T. Farkhondeh, F. Shakeri, A. Farshbaf, M. H. Boskabady, The effect of environmental lead exposure on human health and the contribution of inflammatory mechanisms, a review, Environment international 120 (2018) 404–420.

[15] K. Deibler, P. Basu, Continuing issues with lead: Recent advances in detection, European journal of inorganic chemistry 2013 (7) (2013) 1086.

[16] M.Y. Khorasani, H. Langari, S.B.T. Sany, M. Rezayi, A. Sahebkar, The role of curcumin and its derivatives in sensory applications, Materials Science and Engineering: C 103 (2019) 109792.

[17] S. Raj, D.R. Shankaran, Curcumin based biocompatible nanofibers for lead ion detection, Sensors and Actuators B: Chemical 226 (2016) 318–325.

[18] L.Y. Heng, E.A. Hall, Producing "self-plasticizing" ion-selective membranes, Analytical chemistry 72 (1) (2000) 42–51.

[19] L.Y. Heng, E.A. Hall, Assessing a photocured self-plasticised acrylic membrane recipe for Na+ and K+ ion selective electrodes, Analytica Chimica Acta 443 (1) (2001) 25–40.

[20] E. Malinowska, L. Gawart, P. Parzuchowski, G. Rokicki, Z. Brzózka, Novel approach of immobilization of calix [4] arene type ionophore in 'self-plasticized'polymeric membrane, Analytica Chimica Acta 421 (1) (2000) 93–101.

[21] L.Y. Heng, S. Alva, M. Ahmad, Ammonium ion sensor based on photocured and self-plasticising acrylic films for the analysis of sewage, Sensors and Actuators B: Chemical 98 (2–3) (2004) 160–165.

[22] J. Jumal, B.M. Yamin, M. Ahmad, L.Y. Heng, Mercury ion-selective electrode with self-plasticizing poly (n–buthylacrylate) membrane based on 1, 2-bis-(n'–benzoylthioureido) cyclohexane as ionophore, APCBEE Procedia 3 (2012) 116–123.

[23] N.R. Said, M. Rezayi, L. Narimani, N.N. Al-Mohammed, N.S.A. Manan, Y. Alias, A New N-Heterocyclic Carbene Ionophore in Plasticizer-free Polypyrrole Membrane for Determining Ag+ in Tap Water, Electrochimica Acta 197 (2016) 10–22.

[24] A.A. Abraham, M. Rezayi, N.S. Manan, L. Narimani, A.N.B. Rosli, Y. Alias, A novel potentiometric sensor based on 1, 2-Bis (N'-benzoylthioureido) benzene and reduced graphene oxide for determination of lead (II) cation in raw milk, Electrochimica Acta 165 (2015) 221–231.

[25] Y. Umezawa, K. Umezawa, H. Sato, Selectivity coefficients for methods for reporting Krb values ion-selective electrodes: recommended, Pure Appl. Chem. 67 (1995) 507–518.

[26] W.J. Hehre, Ab initio molecular orbital theory, Accounts of Chemical Research 9 (11) (1976) 399–406.

[27] C. Gonzalez, H. Schlegel, Steepest descent path following, J. Chem. Phys 94 (1990) 5523.

[28] C. Gonzalez, H.B. Schlegel, An improved algorithm for reaction path following, The Journal of Chemical Physics 90 (4) (1989) 2154–2161.

[29] A. Klamt, G. Schüürmann, COSMO: a new approach to dielectric screening in solvents with explicit expressions for the screening energy and its gradient, Journal of the Chemical Society, Perkin Transactions 2 (5) (1993) 799–805.

[30] J. Andzelm, C. Kölmel, A. Klamt, Incorporation of solvent effects into density functional calculations of molecular energies and geometries, The Journal of chemical physics 103 (21) (1995) 9312–9320.

[31] V. Barone, M. Cossi, Quantum calculation of molecular energies and energy gradients in solution by a conductor solvent model, The Journal of Physical Chemistry A 102 (11) (1998) 1995–2001.

[32] M. Cossi, N. Rega, G. Scalmani, V. Barone, Energies, structures, and electronic properties of molecules in solution with the C-PCM solvation model, Journal of computational chemistry 24 (6) (2003) 669–681.

[33] T. Lu, F. Chen, Multiwfn: a multifunctional wavefunction analyzer, Journal of computational chemistry 33 (5) (2012) 580–592.

[34] H. Ibrahim, Y.M. Issa, O.R. Shehab, New selenite ion-selective electrodes based on 5,10,15,20-tetrakis-(4-methoxyphenyl)-21H,23H-porphyrin-Co(II), Journal of Hazardous Materials 181 (1–3) (2010).

[35] H.R. Pouretedal, M.H. Keshavarz, Lead (II)-selective electrode based on dibenzodiaza-15-crown-4, Asian Journal of Chemistry 16 (3) (2004) 1319.

[36] A. Abbaspour, F. Tavakol, Lead-selective electrode by using benzyl disulphide as ionophore, Analytica chimica acta 378 (1–3) (1999) 145–149.

[37] A. Rouhollahi, M.R. Ganjali, M. Shamsipur, Lead ion selective PVC membrane electrode based on 5, 5′-dithiobis-(2-nitrobenzoic acid), Talanta 46 (6) (1998) 1341–1346.

[38] D. Wilson, M. de los Ángeles Arada, S. Alegret, and M. del Valle, "Lead (II) ion selective electrodes with PVC membranes based on two bis-thioureas as ionophores: 1, 3-bis (N′-benzoylthioureido) benzene and 1, 3-bis (N′-furoylthioureido) benzene," *Journal of hazardous materials,* vol. 181, no. 1-3, pp. 140-146, 2010.

[39] S. Kamata, K. Onoyama, Lead-selective membrane electrode using methylene bis (diisobutyldithiocarbamate) neutral carrier, Analytical chemistry 63 (13) (1991) 1295–1298.

[40] H.K. Lee, K. Song, H.R. Seo, Y.-K. Choi, S. Jeon, Lead (II)-selective electrodes based on tetrakis (2-hydroxy-1-naphthyl) porphyrins: the effect of atropisomers, Sensors and Actuators B: Chemical 99 (2–3) (2004) 323–329.